Theoretical study on the piezoelectric performance of lead-free 1–3-type composites

Vitaly Yu. Topolov[*, 1,2], Christopher R. Bowen[3], Ashura N. Isaeva[1,4], and Alexander A. Panich[2]

[1] Department of Physics, Southern Federal University, 5 Zorge street, 344090 Rostov-on-Don, Russia
[2] Institute of High Technologies and Piezotechnics, Southern Federal University, 10 Milchakov street, 344090 Rostov-on-Don, Russia
[3] Department of Mechanical Engineering, University of Bath, BA2 7AY Bath, UK
[4] IRC "Smart Materials", Southern Federal University, 178 / 24 Sladkova street, 344090 Rostov-on-Don, Russia

Received 2017, revised , accepted
Published online ZZZ

Keywords piezo-active composite; lead-free component; piezoelectric coefficient; sensitivity; anisotropy

[*] Corresponding author: e-mail vutopolov@sfedu.ru, Phone: +07 903 470 17 09, Fax: +07 863 297 51 20,
Web: www.phys.sfedu.ru

The paper is devoted to the analysis of high-performance piezo-composites based on lead-free ferroelectric single crystals. The composite consists of parallelepiped-shaped single-crystal rods which are surrounded by a laminar polymer matrix, and the composite as a whole is described by 1–2–2 connectivity. Such a composite structure promotes high piezoelectric sensitivity and hydrostatic response. Of particular interest are piezoelectric coefficients g_{33}^* and h_{33}^*, squared figure of merit $d_{33}^* g_{33}^*$, electromechanical coupling factor k_t^* at the thickness-mode oscillation, and hydrostatic parameters g_h^* and $d_h^* g_h^*$. The influence of the laminar matrix on the aforementioned parameters is studied in a wide volume-fraction range. Examples of maxima and large anisotropy of some effective parameters are discussed for the 1–2–2 composites based on $[Li_x(K_{1-y}Na_y)_{1-x}](Nb_{1-z}Ta_z)O_3$:Mn single crystals. The role of elastic properties of the laminar matrix in achieving large hydrostatic parameters and piezoelectric anisotropy of these composites is emphasised. Their effective parameters are compared to those of composites based on the lead-containing relaxor-ferroelectric single crystals and to specific parameters of poled textured ceramics. Advantages of the studied composites over the relaxor-ferroelectric-based composites and textured ceramics open up new possibilities to apply the 1–3-type lead-free composites as active elements of piezoelectric sensors, hydrophones, energy-harvesting, and transducer devices.

1 Introduction

As is known from the literature, the overwhelming majority of ferroelectrics (FE) ceramics and single crystals (SCs) which exhibit high electromechanical coupling and important physical properties are lead-containing materials [1, 2] which unfortunately have the potential to pollute the environment. Research trends to discover an appropriate alternative to lead-containing FE and piezoelectric materials have been important in the last decade [3–6]. Among the promising materials that can be used as lead-free FEs are polycrystalline ceramics and SCs based on alkali niobates. For instance, the longitudinal piezoelectric coefficient d_{33} of various poled (K, Na, Li)(Nb, Ta, Sb)O_3 [3], (K, Na, Li)(Nb, Sb)O_3 [5], (K, Li)(Nb, Ta, Sb)O_3 [6] and (K, Na)NbO_3-based [4] ceramics can be found in the range from ~ 200 pC N^{-1} to 300 pC N^{-1} at room temperature. In poled samples of textured (K, Na, Li)(Nb, Ta, Sb)O_3 ceramics, the value of d_{33} = 416 pC N^{-1} [3] is achieved. A ferroelectric nanostructured Mn-modified $(K_{0.5}Na_{0.5})NbO_3$ ceramic is characterised by the piezoelectric coefficients d_{33} = 340 pC N^{-1}

and g_{33} = 220 mV·m·N^{-1} and an anisotropy factor $d_{33}/|d_{31}| \approx 21$ [7]. Of independent interest are domain-engineered FE SCs based on alkali niobates-tantalates with optimised electromechanical properties. These SCs are characterised [8–10] by relatively large piezoelectric coefficients d_{ij} and electromechanical coupling factors k_{ij}. For example, the piezoelectric coefficients of some (K, Na, Li)(Nb, Ta)O_3-based SCs [10] poled along the perovskite unit-cell [001] direction exceed the typical values of $d_{33} \approx 400$–500 pC N^{-1} and $g_{33} \approx 30$–40 mV·m·N^{-1} of numerous FE ceramics based on Pb(Zr, Ti)O_3 [1, 11] with compositions near the morphotropic phase boundaries. However the aforementioned d_{33} values are smaller than those of domain-engineered relaxor-FE SCs such as $(1-x)$Pb$(Mg_{1/3}Nb_{2/3})O_3 - x$PbTi$O_3$ (PMN–xPT) and $(1-x)$Pb$(Zn_{1/3}Nb_{2/3})O_3 - x$PbTi$O_3$ [12, 13]. Examples of full sets of electromechanical constants of the [001]-poled lead-free $[Li_x(K_{1-y}Na_y)_{1-x}](Nb_{1-z}Ta_z)O_3$:Mn and lead-containing PMN–0.33PT SCs are shown in Table 1. We add that both the SC compositions are located close to the morphotropic phase boundary.

An example of using the domain-engineered lead-free SC as an active component of a 1–3-type composite was first discussed in work [18] where a high piezoelectric sensitivity associated with the piezoelectric coefficients g_{33}^* and g_h^* and related figures of merit was highlighted. We remind the reader that 1–3 connectivity in a piezo-active composite [19] relates to the presence of a system of long aligned piezoelectric rods (continuous along one co-ordinate axis) in a large matrix (continuous along three co-ordinate axes). The piezoelectric performance of a lead-free 1–3 ceramic / polymer composite studied in work [20] showed that such a material is of interest due to its electromechanical coupling factor k_t^*, piezoelectric coefficient g_{33}^*, and acoustic impedance Z^*. The ferroelectric ceramic used to form the piezoelectric rods of the 1–3 composite had a nominal composition expressed by the formula $(Na_{0.535}K_{0.485})_{0.914}Li_{0.086}(Nb_{0.942}Ta_{0.058})O_3$ [20].

A modification of the 1–3 composite structure, especially the matrix surrounding the piezoelectric rods, may lead to improved parameters, see, e.g. Refs. 15, 21 and 22. To the best of our knowledge, lead-free 1–3-type composites have yet to be studied in the context of the improvement of their parameters for potential piezotechnical applications. It is also important and timely to show advantages of the lead-free composites over their lead-containing counterparts such as 1–3-type composites based on PMN–xPT SCs [23]. Below we discuss the role of the SC and polymer components in forming the piezoelectric performance and hydrostatic response of the 1–3-type composite wherein the matrix exhibits specific elastic properties.

2 Model of the composite, its components and effective properties

In our study, the 1–3-type composite contains a system of ferroelectric domain-engineered SC rods in the form of rectangular parallelepipeds with square bases (Fig. 1). These parallelepipeds are continuous in the OX_3 direction, and their lateral faces are parallel to the (X_1OX_3) and (X_2OX_3) planes. It is assumed that each SC rod poled along the [001] direction of the perovskite unit cell is split into domains with spontaneous polarisation vectors $\boldsymbol{P}_{s,1}$, $\boldsymbol{P}_{s,2}$, $\boldsymbol{P}_{s,3}$, and $\boldsymbol{P}_{s,4}$, see the inset 1 of Fig. 1. The main crystallographic axes X, Y and Z of each SC rod are oriented as follows: X || OX_1, Y || OX_2 and Z || $\boldsymbol{P}_s^{(1)}$ || OX_3, where $\boldsymbol{P}_s^{(1)}$ is the spontaneous polarisation of the SC rod (or component as a whole), and OX_3 is the poling axis for the composite sample. The SC rods are regularly distributed in the polymer matrix so that the centres of symmetry of the rod bases

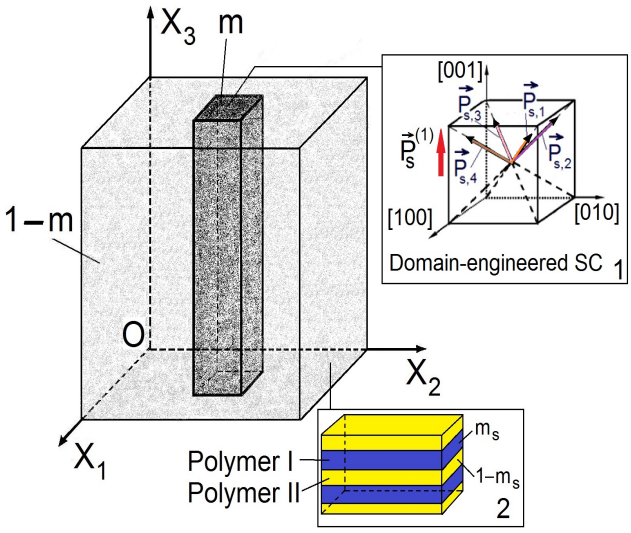

Figure 1 Schematic of the 1–2–2 SC / *polymer I* / *polymer II* composite with the planar microgeometry. ($X_1X_2X_3$) is the rectangular co-ordinate system, m is the volume fraction of the SC component, and m_s is the volume fraction of polymer I in the laminar matrix

form a simple square lattice in the (X_1OX_2) plane. The matrix that surrounds the SC rods consists of two polymer components, i.e., *polymer I* and *polymer II* in the form of layers with interfaces that are parallel to the (X_1OX_2) plane, see the inset 2 in Fig. 1. These layers are distributed regularly along the OX_3 axis. Hereafter we use the term '*polymer I*' to denote a component with a larger stiffness, and the term '*polymer II*' is related to a component with a smaller stiffness in the laminar matrix. This matrix is characterised by 2–2 connectivity in terms of work [19, 21], and the 1–3-type composite as a whole is characterised by 1–2–2 connectivity. It is assumed that electrodes applied to the composite sample shown in Fig. 1 are parallel to the (X_1OX_2) plane.

The effective properties of the 1–2–2 composite are determined by means of the matrix method [14, 20, 21]. In the first stage, this method is applied to the laminar matrix, and boundary conditions for components of mechanical and electric fields [20] are taken into account at interfaces x_3 = const. The averaging procedure is carried out for the properties of the polymer components, and the effective properties of the laminar matrix depend on a volume fraction m_s of *polymer I*. In the second stage, the averaging procedure is performed for the system "rods – matrix", and the aforementioned boundary conditions are applied to interfaces x_1 = const and x_2 = const (Fig. 1) by taking into account the boundary conditions described in monograph [20]. The volume fraction of SC, m, is a parameter on which the properties are now averaged. Such an averaging procedure is performed under the condition that the thickness of each polymer layer of the matrix is much smaller than the linear sizes of the SC rod base in the (X_1OX_2) plane, i.e., the system of the SC rods is surrounded by a laminar matrix with the effective (or homogenised) properties that have been determined in the first stage.

As a result of averaging, we find the effective electromechanical properties of the 1–2–2 composite. In the present study, these properties are characterised by the effective piezoelectric coefficients d_{ij}^*, elastic compliances s_{ab}^{*E} at electric field E = const and dielectric permittivities $\varepsilon_{pp}^{*\sigma}$ at mechanical stress σ = const. Hereafter with the asterisk (*), we denote the effective properties and parameters of the studied composite. We remind the reader that the aforementioned properties are involved in the following equations of a piezoelectric medium [20, 24]:

$$\xi_a = s_{ab}^{*E}\sigma_b + d_{ia}^* E_i \text{ and } D_i = d_{ij}^*\sigma_j + \varepsilon_{ir}^{*\sigma} E_r. \quad (1)$$

In Eqs. (1), ξ_a, σ_b, E_i, and D_i are mechanical strain, mechanical stress, electric field, and electric displacement, respectively.

The effective properties from Eqs. (1) and related parameters of the 1–2–2 composite are regarded as functions of the volume fractions m and m_s, and they can be varied in the range from 0 to 1. At m_s = 0 or 1, we obtain

a 1–3 SC / polymer composite whose effective properties were studied earlier; see, e.g. Refs. 21 and 23.

The components that are of interest for our analysis and comparison are shown in Table 1, and their electromechanical constants are used in our evaluations. The lead-free KNNTL:Mn SC is of particular interest due to the large piezoelectric coefficients g_{ij} and h_{ij} and planar electromechanical coupling factor (ECF) k_p. It is seen from data in Table 1 that an unusual piezoelectric anisotropy is observed, i.e., conditions

$$| e_{31} | > e_{33} \text{ and } | h_{31} | > h_{33} \quad (2)$$

hold for the KNNTL:Mn SC at the relatively small ratio $d_{33} / | d_{31} | = 2.10$; as shown by the data in Table 1. The PMN–0.33PT SC is regarded as a highly piezo-active lead-containing counterpart whose piezoelectric properties are characterised by validity of the condition

$$e_{33} / | e_{31} | = h_{33} / | h_{31} | > 5 \quad (3)$$

at $d_{33} / | d_{31}| = 2.12$ (see data Table 1). We also consider three piezo-passive isotropic polymers as components of the laminar matrix. Hereby polyethylene (PE) is the softest component of the laminar matrix and will be regarded as *polymer II* in our further analysis.

Taking into account the effective properties of the composite $d_{ij}^*(m, m_s)$, $s_{ab}^{*E}(m, m_s)$ and $\varepsilon_{pp}^{*\sigma}(m, m_s)$, we evaluate the effective piezoelectric coefficients $g_{ij}^*(m, m_s)$, $e_{ij}^*(m, m_s)$, and $h_{ij}^*(m, m_s)$, and related parameters in accordance with formulae [20, 22]. In Section 3 we consider some examples of large parameters and specifics of their volume-fraction behaviour in the lead-free 1–2–2 composites.

3 Large effective parameters of 1–2–2 composites

3.1 Piezoelectric coefficients g_{3j}^* and g_h^*

The piezoelectric sensitivity of composites is often described in terms of their piezoelectric coefficients g_{ij}^* that link [24] an external mechanical stress field and an electric field due to a piezoelectric polarisation. As follows from our study, the presence of a laminar polymer matrix in the 1–2–2 composite (Fig. 1) influences the piezoelectric coefficients g_{3j}^* and their hydrostatic analog

$$g_h^* = g_{31}^* + g_{32}^* + g_{33}^*. \quad (4)$$

Taking into account the microgeometry and macroscopic symmetry of the studied 1–2–2 composite, we represent its piezoelectric coefficients from Eq. (4) as

$$g_{3j}^* = d_{3j}^* / \varepsilon_{33}^{*\sigma} \text{ and } g_h^* = d_h^* / \varepsilon_{33}^{*\sigma},$$

Table 1 Room-temperature elastic compliances s_{ab}^E (in 10^{-12} Pa^{-1}), piezoelectric coefficients d_{ij} (in pC / N) and relative dielectric permittivity $\varepsilon_{pp}^{\sigma} / \varepsilon_0$ of [001]-poled domain-engineered KNNTL:Mn[a] [10] and PMN–0.33PT [13] SCs, araldite [14], polyurethane [15], and polyethylene[b] [16, 17]

Components	s_{11}^E	s_{12}^E	s_{13}^E		s_{44}^E	s_{66}^E	d_{31}	d_{33}	d_{15}	$\varepsilon_{11}^{\sigma} / \varepsilon_0$	$\varepsilon_{33}^{\sigma} / \varepsilon_0$
KNNTL:Mn SC	33.4	–7.36	–25.8	57.7	12.8	13.5	–260	545	66	400	650
PMN–0.33PT SC[c]	69.0	–11.1	–55.7	119.6	14.5	15.2	–1330	2820	146	1600	8200
Araldite	216	–78	–78	216	588	588	0	0	0	4.0	4.0
Polyurethane	401	–149	–149	401	1100	1100	0	0	0	3.5	3.5
Polyethylene	1430	–286	–286	1430	3430	3430	0	0	0	2.3	2.3

[a] $[Li_x(K_{1-y}Na_y)_{1-x}](Nb_{1-z}Ta_z)O_3$:Mn, where $x = 0.06$, $y = 0.1–0.3$, $z = 0.07–0.17$, and the level of Mn doping is 0.25 mol. %, see Ref. 10.

This SC is characterised by 4*mm* symmetry, piezoelectric coefficients $g_{33} = 94.7$ and $g_{31} = –45.2$ (in mV·m·N^{-1}), $e_{33} = 4.53$ and $e_{31} =$ –5.50 (in C·m^{-2}), $h_{33} = 106$ and $h_{31} = –129$ (in 10^8 V·m^{-1}), squared figure of merit $d_{33}g_{33} = 51.6 \cdot 10^{-12}$ Pa^{-1}, and electromechanical coupling factors $k_t = 0.491$ (thickness oscillation mode) and $| k_p | = 0.951$ (planar oscillation mode).

[b] Elastic properties of monolithic polyethylene are taken from work [16], and dielectric properties are taken from work [17].

[c] This SC is characterised by 4*mm* symmetry, piezoelectric coefficients $g_{33} = 38.9$ and $g_{31} = –18.3$ (in mV·m·N^{-1}), $e_{33} = 20.3$ and $e_{31} =$

(5)

where j = 1, 2 and 3, and $d_h^* = d_{31}^* + d_{32}^* + d_{33}^*$. We add that equalities $d_{31}^* = d_{32}^*$ and $g_{31}^* = g_{32}^*$ hold because of the regular distribution of the SC rods from the 4*mm* symmetry class in the laminar polymer matrix with ∞*mm* symmetry, and therefore, the hydrostatic piezoelectric coefficients from Eqs. (4) and (5) can be written as $d_h^* = d_{33}^* + 2\,d_{31}^*$ and $g_h^* = g_{33}^* + 2\,g_{31}^*$.

The piezoelectric coefficients g_{3j}^* and g_h^* are characterised by extremum points at volume fractions of SC m << 1 (Figs. 2 and 3), and this is a common feature of 1–3-type piezo-active composites [22, 23]. Such a feature is a result of the strong influence of the dielectric permittivity $\varepsilon_{33}^{*\sigma}$ from Eqs. (5) on g_{3j}^* and g_h^* at small volume fractions of SC, i.e., when its dielectric properties make a very small contribution to $\varepsilon_{33}^{*\sigma}$ and when the piezoelectric coefficients d_{3j}^* undergo considerable changes (e.g. rapid increase of d_{33}^* on increasing the volume fraction of SC) [21, 23] due to the system of the parallel SC rods in the relatively soft matrix. In Figs. 2 and 3 we do not present the behaviour of the piezoelectric coefficient g_{31}^* since it may be simply evaluated from the expression $g_{31}^* = (g_h^* - g_{33}^*) / 2$. In the 2D graphs shown in Figs. 2, d and e and 3, e, we show the behaviour of g_h^* near local max g_h^* at m_s = const.

As follows from our data, local min g_{31}^* is achieved almost at a volume fraction m related to local max g_{33}^* at m_s = const (Figs. 2, a and 3, a). It is seen from Fig. 2, b that a diffuse max g_h^* is observed at m < 0.02 and 0.05 < m_s < 0.15, and decrease in g_h^* is related to an increase of the volume fraction of SC m. On comparing the hydrostatic piezoelectric coefficients g_h^* of the araldite- and polyurethane-containing composites, we observe that the larger max g_h^* value is related to the araldite-containing composite, see Figs. 2, b and 3, b and data in Table 2. This is achieved despite the larger values of g_{33}^* in the polyurethane-containing composite (see Figs. 2, a and c, 3, a and c, and the 4th column in Table 2). The laminar matrix (inset 2 in Fig. 1), wherein the elastic properties of the polymer components differ to a smaller degree, promotes a larger piezoelectric coefficient g_{33}^* at m = const. Data on polymers from Table 1 suggest that a smaller difference is expected for the composite with the polyurethane / PE matrix. Data in Table 2 show that a difference between the g_{33}^* values calculated for the related composites at m_s = const and m = const can reach a few percent. However the g_{31}^* values calculated for the same composites at m_s = const and m = const can differ to a larger extent (see data in the 5th column of Table 2). For example, at m_s = 0.05 and m = 0.012 we see a 1% difference between g_{33}^* and a 14% difference between g_{31}^* of the studied 1–2–2 composites. On moving away from the max g_h^* point we also observe a considerable difference between the g_{31}^* values. For instance, at m_s = 0.10 and m = 0.050 this difference reaches 19% since almost equal g_{33}^* values of the same com-

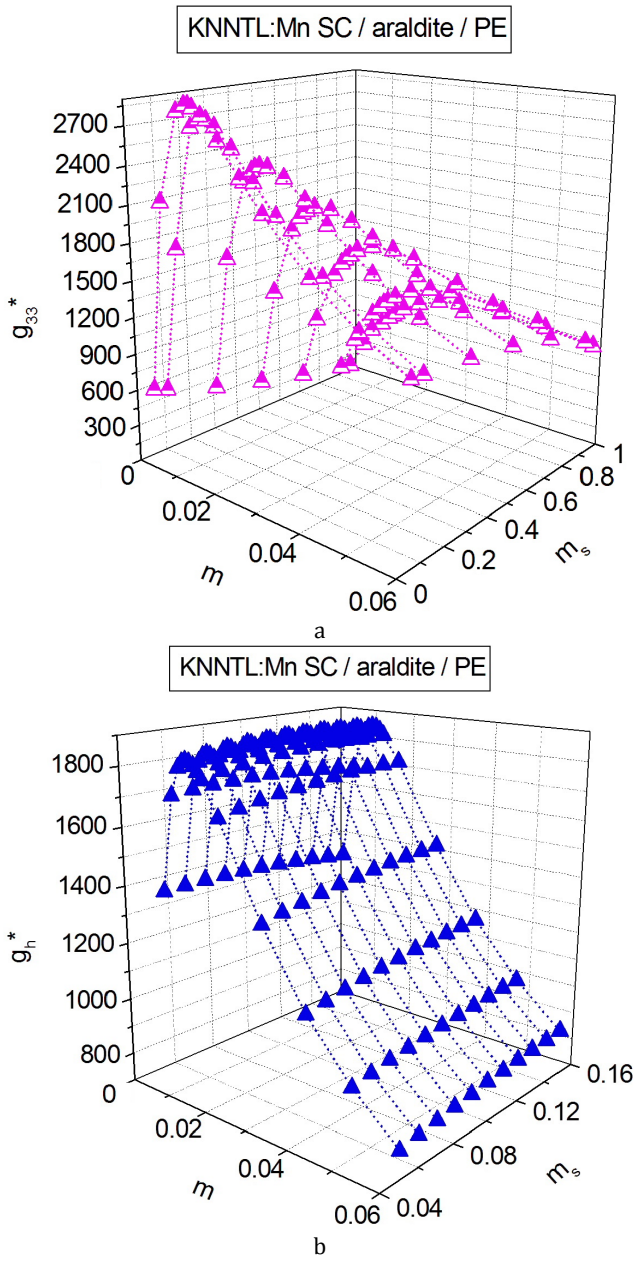

Figure 2 Volume-fraction behaviour of the piezoelectric coefficients g_{33}^* (a and c, in mV·m·N^{-1}) and g_h^* (b, d and e, in mV·m·N^{-1}) of the 1–2–2 KNNTL:Mn SC / araldite / PE composite near local max g_{33}^* and max g_h^*, and relations between g_{3j}^* and g_h^* (f, in mV·m·N^{-1}) at volume fractions of SC m = 0.05 (curves 1–3 in graph f) and m = 0.10 (curves 4–6 in graph f).

posites are observed. Data from Table 2 suggest that in the araldite-containing composite (with the larger difference between the elastic properties of polymers), a smaller contribution from $|g_{31}^*|$ into g_h^* is observed at m_s = const. This can lead to a larger g_h^* value even with a smaller contribution from g_{33}^* in Eq. (4). In our opinion, the transverse piezoelectric effect in the 1–2–2 composite plays the important role in forming the hydrostatic piezoelectric res-

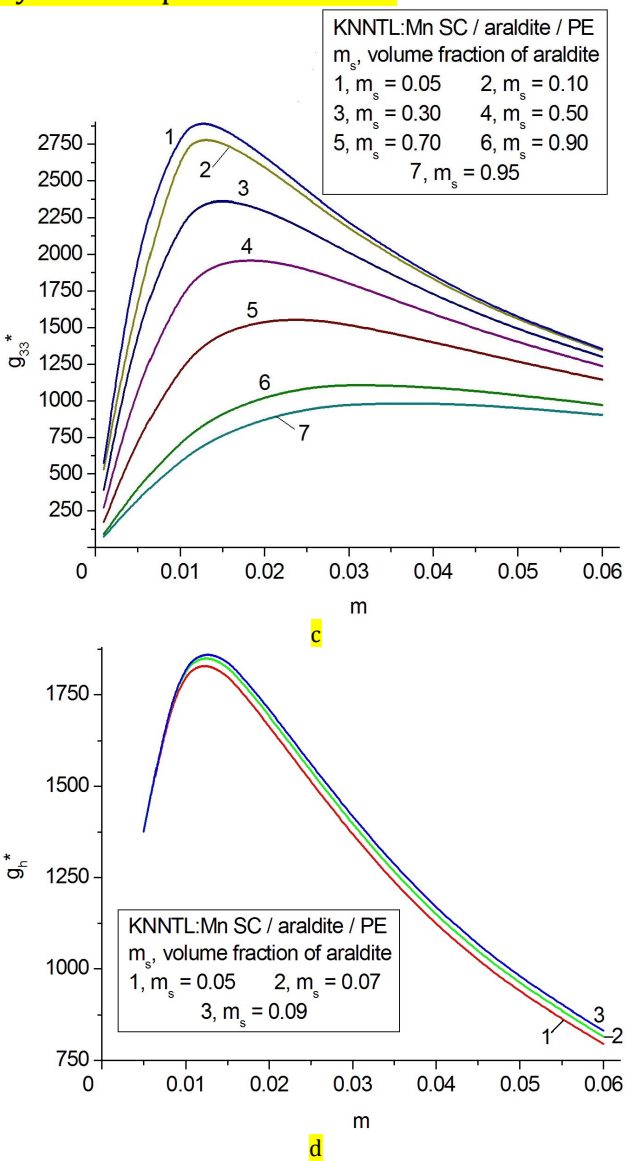

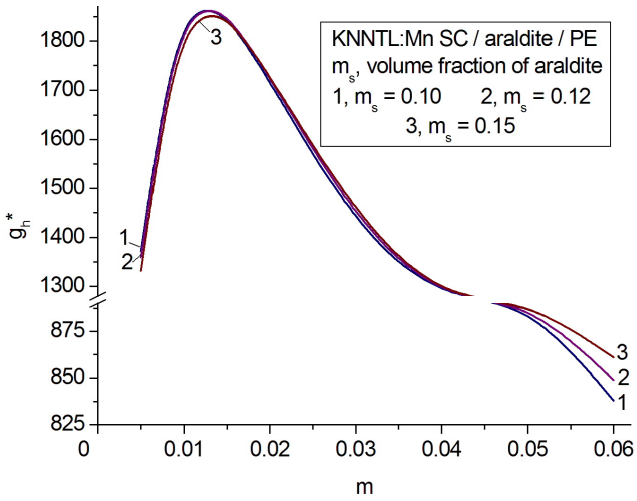

e

Figure 2 (continued)

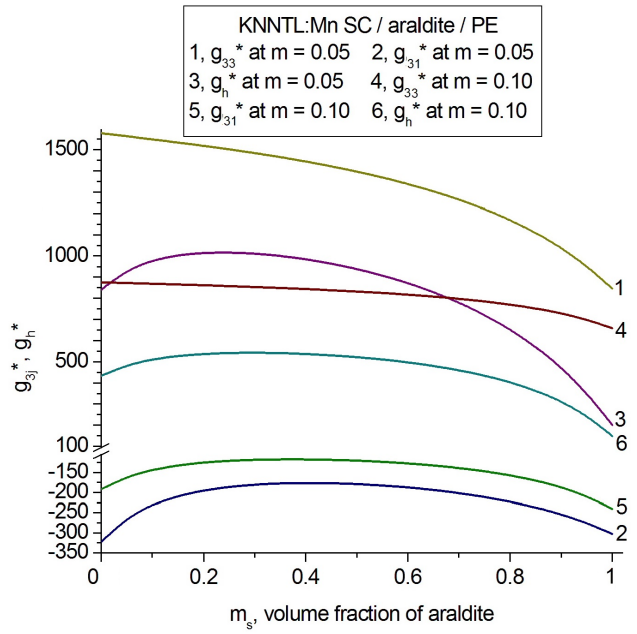

f

Figure 2 (continued)

ponse, and this role is inseparably linked with the anisotropic elastic properties of the laminar matrix that influences mechanical and electric fields in the piezoelectric SC rods. We add that some features of these elastic properties will be discussed in Section 3.3.

The need for small volume fractions of SC *m* may be problematic in terms of ease of manufacturing of composites with the stable piezoelectric performance. Data on 1–3 ferroelectric ceramic / polymer composites have been reported in the literature, where Choy et al. [25] manufactured the samples with low volume fractions of FE ceramic rods (approximately 0.033, 0.066 etc.), and therefore, the 1–3-type composite with volume fractions of SC $0.03 < m < 0.1$ (Fig. 1) could be manufactured. To compare the piezoelectric coefficients from Eqs. (5), we consider the performance of the 1–2–2 composites based on the KNNTL:Mn SC at m = 0.05 and 0.10. The graphs in Fig. 2, d–f and 3, d and e show that a considerable dependence of g_h^* and g_{3j}^* on the volume fraction of *polymer I* m_s is observed even at the volume fractions of SC $m \le 0.10$. This means that the elastic anisotropy of the laminar matrix plays an important role in forming the piezoelectric sensitivity of the composite and, therefore, can influence its piezoelectric anisotropy. It should be added that local max g_h^* at m = 0.05 can be found in the volume-fraction range $0.2 < m_s < 0.3$ for both the composites, see curves 3 in Figs. 2, f and 3, e.

3.2 Squared figures of merit $(Q_{3j}^*)^2$ and $(Q_h^*)^2$

Squared strain–voltage figures of merit

$$(Q_{33}^*)^2 = d_{33}^* g_{33}^* \text{ and } (Q_{31}^*)^2 = d_{31}^* g_{31}^* \quad (6)$$

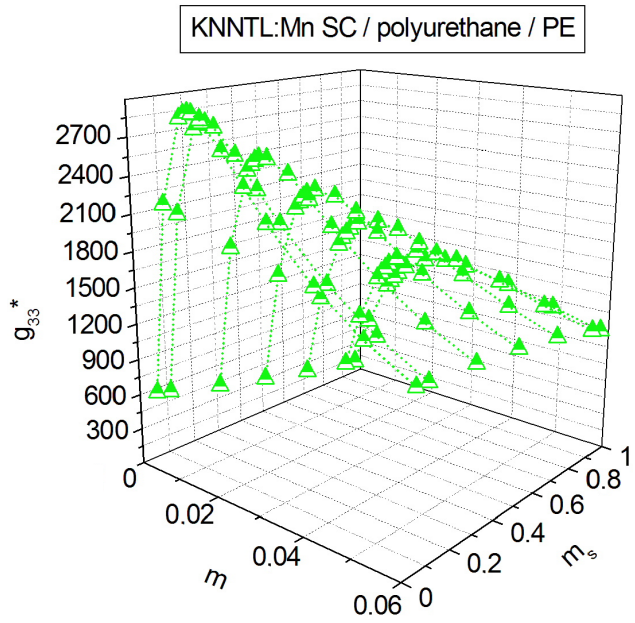

a

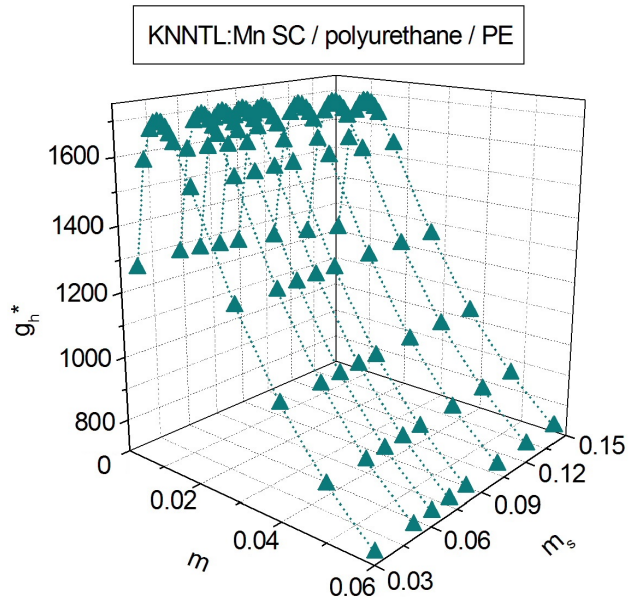

b

Figure 3 Volume-fraction behaviour of the piezoelectric coefficients g_{33}^* (a and c, in mV·m·N^{-1}) and g_h^* (b and d, in mV·m·N^{-1}) of the 1–2–2 KNNTL:Mn SC / polyurethane / PE composite near local max g_{33}^*, and relations between g_{3j}^* and g_h^* (e, in mV·m·N^{-1}) at volume fractions of SC m = 0.05 (curves 1–3 in graph e) and m = 0.10 (curves 4–6 in graph e).

are concerned with the longitudinal and transverse piezoelectric effect, respectively. The hydrostatic analog of the parameters from Eqs. (6) is written in terms of the hydrostatic piezoelectric coefficients d_h^* and g_h^* from Eqs. (5) as follows:

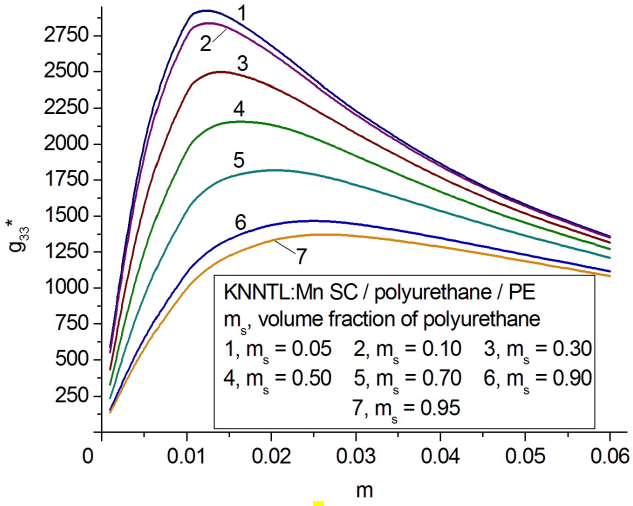

c

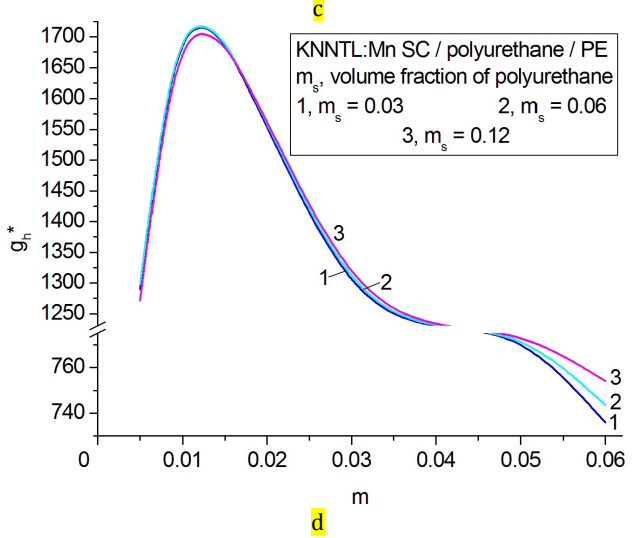

d

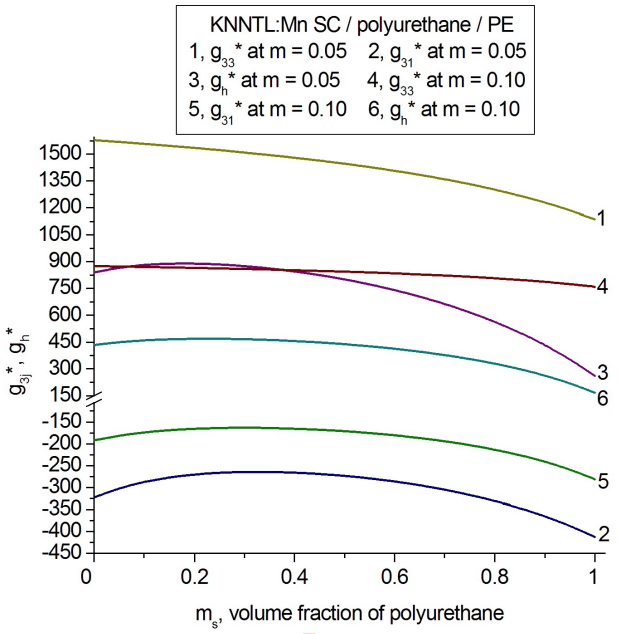

e

Figure 3 (continued)

Table 2 Piezoelectric coefficients g_h^* and g_{3j}^* (in mV·m·N^{-1}) of the 1–2–2 KNNTL:Mn SC / araldite / PE and KNNTL:Mn SC / polyurethane / PE near local max g_h^*

m_s	m	g_h^*	g_{33}^*	g_{31}^*
KNNTL:Mn SC / araldite / PE composite				
0.05	0.012[a]	1830	2890	–530
0.08	0.012[a]	1860	2820	–480
0.10	0.013[a]	1860	2780	–460
	0.030	1420	2170	–375
	0.050	980	1550	–285
0.14	0.013[a]	1860	2690	–415
0.18	0.013[a]	1830	2610	–390
KNNTL:Mn SC / polyurethane / PE composite				
0.05	0.012[a]	1720	2930	–605
0.07	0.012[a]	1720	2890	–585
0.10	0.012[a]	1710	2840	–565
	0.030	1280	2200	–460
	0.050	883	1560	–339
0.14	0.013[a]	1690	2770	–540
0.16	0.013[a]	1660	2710	–525

[a] The m value at which local max g_h^* is achieved

$$(Q_h^*)^2 = d_h^* g_h^* = (g_h^*)^2 \varepsilon_{33}^{*\sigma}. \quad (7)$$

The squared figures of merit from Eqs. (6) and (7) are used to estimate the sensor signal-to-noise ratio of the composite and its piezoelectric sensitivity [18, 21, 22]. Examples of the volume-fraction behaviour of the squared figures of merit of the studied composites are graphically represented in Fig. 4.

Our comparison of Fig. 4, a to Fig. 2, f and Fig. 4, b to Fig. 3, e shows that there is a correlation between the piezoelectric coefficient g_{33}^* and the squared figure of merit $(Q_{33}^*)^2$ from Eqs. (6) as well a correlation between g_h^* and $(Q_h^*)^2$ from Eq. (7). We see the non-monotonic dependences of both g_h^* and $(Q_h^*)^2$ on the volume fraction m_s. It seems probable that the piezoelectric coefficients g_{3j}^* play a dominating role in the determination of the figures merit from Eqs. (6) and (7) at SC volume fractions of $m \le 0.10$, i.e., at relatively small dielectric permittivities $\varepsilon_{33}^{*\sigma}$.

Irrespective of the polymer components in the laminar matrix, points of max$[(Q_h^*)^2]$ are located close to the volume fraction $m_s = 0.2$, see curves 2 and 4 in graphs of Fig. 4. As with local max g_h^* at $m \le 0.10$ (see Section 3.1), the larger value of local max$[(Q_h^*)^2]$ is achieved in the presence of the araldite-containing laminar matrix, i.e., at the larger difference between the elastic properties of the polymer components.

The large $(Q_{33}^*)^2$ values that are achieved in the composites at $m \le 0.10$ (see curves 1 and 3 in Fig. 4) are compa-

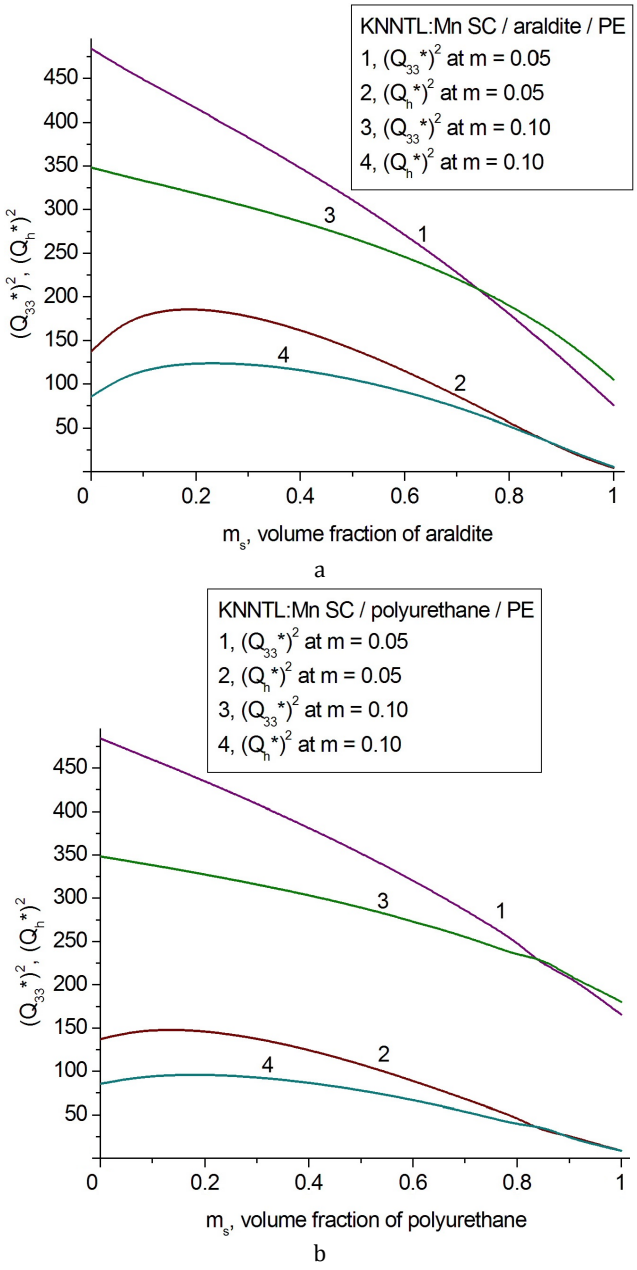

Figure 4 Relations between the squared figures of merit $(Q_{33}^*)^2$ and $(Q_h^*)^2$ (in 10^{-12} Pa^{-1}) of the 1–2–2 KNNTL:Mn SC / araldite / PE (a) and KNNTL:Mn SC / polyurethane / PE (b) composites at volume fractions of SC m = 0.05 (curves 1 and 2) and m = 0.10 (curves 3 and 4).

red to the squared figure of merit $(Q_{31}^*)^2$ (Fig. 5) to find the volume-fraction ranges where the longitudinal piezo-electric sensitivity is dominating. A comparison of curves 1 and 2 in Fig. 5 enables us to determine that the larger anisotropy of the squared figures of merit $(Q_{3j}^*)^2$ from Eqs. (6) is achieved at a smaller volume fraction of SC m and in the volume-fraction range $0.3 < m_s < 0.4$. An increase of m

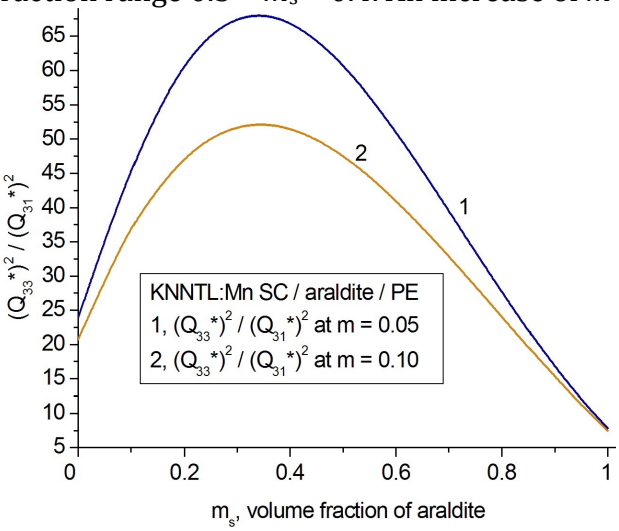

Figure 5 Anisotropy of the squared figures of merit $(Q_{33}^*)^2 / (Q_{31}^*)^2$ of the 1–2–2 KNNTL:Mn SC / araldite / PE composite at volume fractions of SC m = 0.05 (curve 1) and m = 0.10 (curves 2).

leads to the smaller $(Q_{33}^*)^2 / (Q_{31}^*)^2$ ratio, and this is accounted for by the influence of the SC component with a relatively small ratio of the piezoelectric coefficients. We remind the reader that the [001]-poled KNNTL:Mn SC is characterised by the ratio $g_{33} / |g_{31}| = 2.10$, see data in Table 1.

3.3 Elastic properties of the matrix and piezoelectric anisotropy of the composite

In Sections 3.1 and 3.2 we considered the effective parameters of the composite at volume fractions of SC $m \leq 0.10$. In this case, the elastic and dielectric properties of the laminar matrix can influence the electromechanical properties of the composite, its piezoelectric sensitivity, and figures of merit to a large extent.

We start from relations that describe the piezoelectric effect, its anisotropy and hydrostatic response in the composite with 4*mm* symmetry. As seen from Eqs. (5), the

piezoelectric coefficients d_{3j}^* and g_{3j}^* are linked by the dielectric permittivity $\varepsilon_{33}^{*\sigma}$. However, on analysis of the anisotropic piezoelectric effect in the 1–3-type composite, it is easier to use the piezoelectric coefficients e_{3j}^*. As is known from work [21, 26], the 1–3-type composite is characterised by almost linear dependences of e_{3j}^* and $\varepsilon_{33}^{*\sigma}$ on the volume fraction of the piezoelectric rods while this volume fraction remains relatively small. In the same volume-fraction range, the piezoelectric coefficients e_{3j}^* of the composite obey the condition

$$e_{33}^* / |e_{31}^*| >> 1. \qquad (8)$$

The piezoelectric coefficients d_{3j}^* are written in terms of e_{3j}^* [21, 24] as follows:

$$d_{31}^* = e_{31}^* (s_{11}^{*E} + s_{12}^{*E}) + e_{33}^* s_{13}^{*E} \text{ and } d_{33}^* = 2 e_{31}^* s_{13}^{*E} + e_{33}^* s_{33}^{*E}. \qquad (9)$$

Based on Eqs. (5) and (9) and taking into account the condition (8), we represent the hydrostatic piezoelectric coefficients of the composite in the following form:

$$d_h^* \approx e_{33}^* (s_{33}^{*E} + 2 s_{13}^{*E}) \text{ and } g_h^* \approx e_{33}^* (s_{33}^{*E} + 2 s_{13}^{*E}) / \varepsilon_{33}^{*\sigma}. \qquad (10)$$

At the small volume fraction of the piezoelectric rods, the sum $s_{33}^{*E} + 2 s_{13}^{*E}$ from Eqs. (10) will approach the similar sum $s_{33}^{(m)} + 2 s_{13}^{(m)}$ related to the laminar matrix. The anisotropy factor of the composite is then represented as

$$d_{33}^* / |d_{31}^*| = g_{33}^* / |g_{31}^*| \approx s_{33}^{(m)} / |s_{13}^{(m)}|. \qquad (11)$$

Equation (11) enables us to link the piezoelectric anisotropy of the composite and the elastic anisotropy of its laminar matrix.

The elastic properties of the laminar matrix depend on the volume fraction m_s of *polymer I*, see Fig. 6. Of specific interest are curves 3 and 4. It is seen that the elastic compliance $s_{13}^{(m)}$ of both the laminar matrices undergoes considerable changes at $m_s < 0.3$, and $s_{33}^{(m)}$ monotonously decreases in the whole m_s range. Such a behaviour of the elastic compliances $s_{a3}^{(m)}$ (see curves 3 and 4 in Fig. 6) suggests that a compromise m_s range can be found where $|s_{13}^{(m)}|$ remains relatively small and $s_{33}^{(m)}$ remains relatively large. Earlier we mentioned the volume-fraction ranges $0.2 < m_s < 0.3$ and $0.3 < m_s < 0.4$: the first range is concerned with local max g_h^* at $m = 0.05$ (see Section 3.1), and the latter range is concerned with the large anisotropy of the squared figures of merit $(Q_{3j}^*)^2$; see Section 3.2.

Thus, Eq. (11) and Fig. 6 are to be taken into account at the interpretation of the piezoelectric anisotropy in the studied composites based on the KNNTL:Mn SC. An important example of the large piezoelectric anisotropy of these composites is illustrated by Fig. 7. Hereby we consider validity of the following conditions:

$$d_{33}^* / |d_{31}^*| = g_{33}^* / |g_{31}^*| \geq 5 \qquad (12)$$

and

$$k_t^* / |k_p^*| \geq 5. \qquad (13)$$

Conditions (12) and (13) are concerned with the anisotropy factors that are important for energy-harvesting and other piezotechnical applications [27]. In Eq. (13),

$$k_t^* = e_{33}^* / (c_{33}^{*D} \varepsilon_{33}^{*\xi})^{1/2} \qquad (14)$$

and

$$k_p^* = d_{31}^* \sqrt{\frac{2}{\varepsilon_{33}^{*\sigma}(s_{11}^{*E} + s_{12}^{*E})}} \quad (15)$$

are thickness and planar ECFs, respectively. The ECFs from Eqs. (14) and (15) are used to characterise an

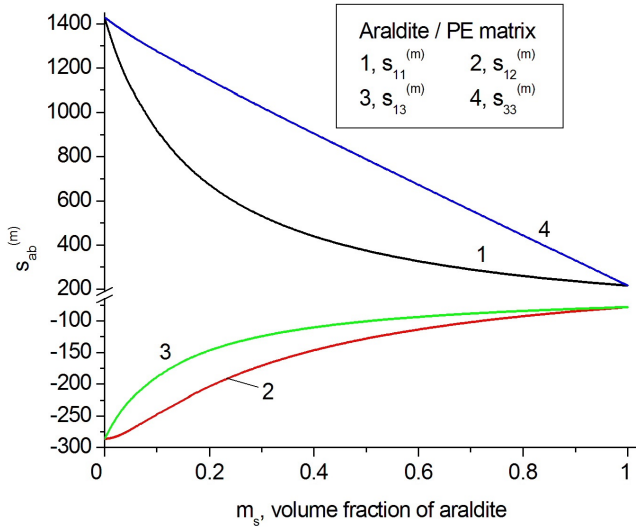

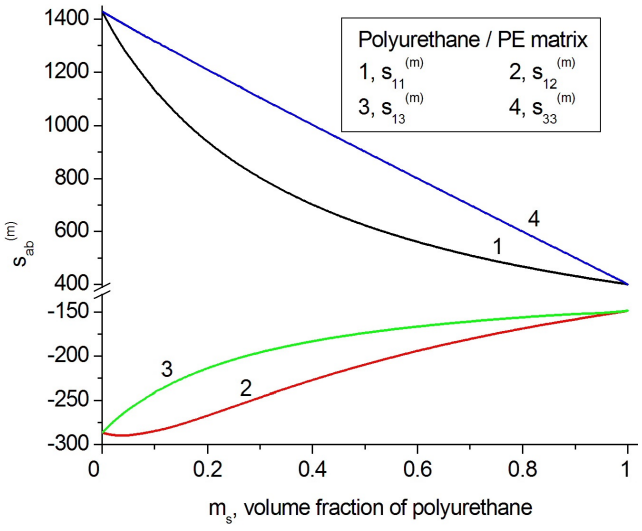

Figure 6 Volume-fraction (m_s) dependence of elastic compliances $s_{ab}^{(m)}$ (in 10^{-12} Pa^{-1}) of the laminar matrix of the composite, see Fig. 1. Graphs a and b are related to the matrices wherein polymer I is araldite and polyurethane, respectively.

effectiveness of the energy conversion in 1–3 composites that are applied as piezo-active elements of transducers [24, 26]. In Eq. (14), c_{33}^{*D} and $\varepsilon_{33}^{*\xi}$ are the elastic modulus at electric displacement D = const and dielectric permittivity at mechanical strain ξ = const, respectively. Based on Eqs. (14) and (15), we represent the ECF anisotropy factor k_t^* / k_p^* as

$$k_t^* / k_p^* = \sqrt{\varepsilon_{33}^{*\sigma}/(2\varepsilon_{33}^{*\xi})}\sqrt{(s_{11}^{*E} + s_{12}^{*E})/c_{33}^{*D}} / s_{13}^{*E}. \quad (16)$$

Taking into account the fact that conditions (12) and (13) to achieve a large piezoelectric anisotropy hold at the relatively small volume fractions m (see area 1 & 2 in Fig. 7, a), we use the following relations to simplify Eq. (16): $s_{ab}^{*E} \approx s_{ab}^{(m)}$ and $c_{33}^{*D} \approx 1 / s_{33}^{(m)}$. After simplification, we write

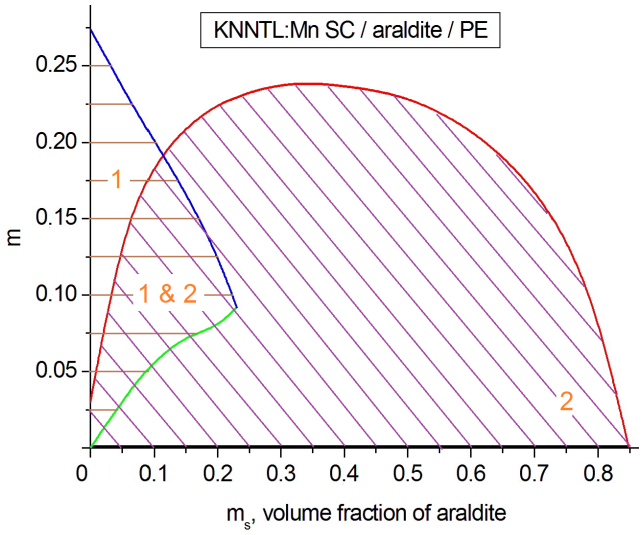

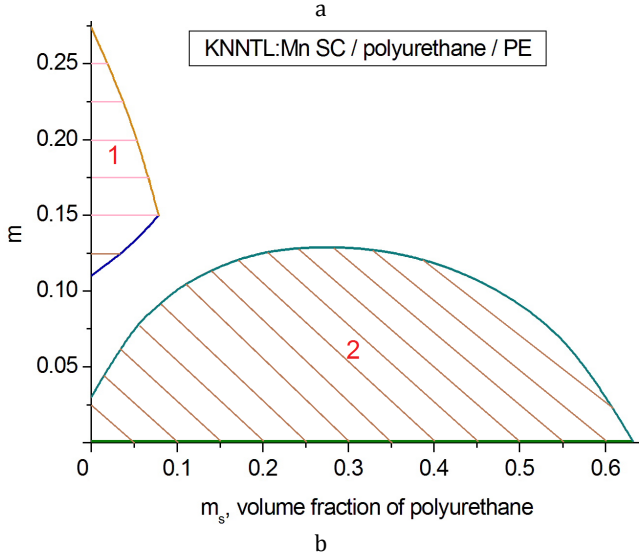

Figure 7 Regions of the large piezoelectric anisotropy in the 1–2–2 KNNTL:Mn SC / araldite / PE (a) and 1–2–2 KNNTL:Mn SC / polyurethane / PE (b) composites: 1, region of the valid condition (13), and 2, region of the valid condition (12).

the ECF anisotropy factor as follows:

$$k_t^* / k_p^* \approx \sqrt{\varepsilon_{33}^{*\sigma} / (2\varepsilon_{33}^{*\xi})}\, s_{anis}, \quad (17)$$

where

$$s_{anis} = \sqrt{(s_{11}^{(m)} + s_{12}^{(m)}) / s_{33}^{(m)}} / s_{13}^{(m)}. \quad (18)$$

Data from Table 3 show that the relations between the elastic compliances of the laminar matrix, namely, s_{anis} from Eq. (18) and $s_{33}^{(m)} / s_{13}^{(m)}$, correlate with the anisotropy factors k_t^* / k_p^* and d_{33}^* / d_{31}^* of the composite, respectively. The $\sqrt{\varepsilon_{33}^{*\sigma} / (2\varepsilon_{33}^{*\xi})}$ factor from Eq. (17) is concerned with the longitudinal dielectric response of the composite and undergoes minor changes at volume fractions $m << 1$ and variations of m_s. A comparison of data from the 3rd and 6th columns of Table 3 enables us to emphasise the key role of the elastic properties of the laminar matrix in achieving a large anisotropy of ECFs from Eq. (16). The s_{anis} factor from Eqs. (17) and (18) enables us to interpret regions 1 in Fig. 7, especially where the interference of regions 1 and 2 is observed (see Fig. 7, a and 5th–7th columns in the first part of Table 3). As in Sections 3.1 and 3.2, we underline the advantage of the araldite-containing composite over the polyurethane-containing composite because conditions (12) and (13) for the large anisotropy hold simultaneously, see the 1 & 2 area in Fig. 7, a. Here it is important to mention the ECF anisotropy factor of the KNNTL:Mn SC for comparison. According to data from Table 1 for this SC, $k_t / |k_p| = 0.516$, i.e., an order-of-magnitude smaller than the k_t^* / k_p^* values related to the araldite-containing composite; see 6th column in the first part of Table 3.

Table 3 Relations between elastic compliances $s_{ab}^{(m)}$ of the laminar matrix[a] and anisotropy factors k_t^* / k_p^* and d_{33}^* / d_{31}^* of the 1–2–2 KNNTL:Mn SC / *polymer I* / *polymer II* composite[b] at the volume fraction of SC $m << 1$

Polymer I / polymer II	Volume fraction of polymer I m_s	s_{anis}, laminar matrix	$s_{33}^{(m)} / s_{13}^{(m)}$, laminar matrix	Volume fraction of SC m	k_t^* / k_p^*, composite	d_{33}^* / d_{31}^*, composite
Araldite / PE	0.05	–4.96	–6.03	0.08	–5.04	–5.63
	0.10	–4.99	–6.83	0.08	–5.09	–6.35
	0.15	–5.00	–7.43	0.08	–5.08	–6.88
	0.20	–5.00	–7.85	0.08	–5.04	–7.25
	0.25	–4.97	–8.12	0.08	–4.88	–7.49
	0.30	–4.90	–8.27	0.08	–4.72	–7.62
Polyurethane / PE	0.05	–4.44	–5.28	0.05	–4.37	–5.20
	0.10	–4.39	–5.48	0.05	–4.30	–5.43
	0.15	–4.31	–5.60	0.05	–4.20	–5.59
	0.20	–4.22	–5.67	0.05	–4.07	–5.69
	0.25	–4.12	–5.69	0.05	–3.95	–5.72
	0.30	–4.01	–5.66	0.05	–3.91	–5.71

[a] See the inset 2 in Fig. 1

3.4 Piezoelectric coefficient h_{33}^* and electromechanical coupling factor k_t^*

The studied 1–2–2 composites based on the KNNTL:Mn SC are also of interest due to large values of the thickness ECF k_t^* from Eq. (14), piezoelectric coefficient

$$h_{33}^* = e_{33}^* / \varepsilon_{33}^{*\xi} \quad (19)$$

and related anisotropy factor $h_{33}^*/|h_{31}^*| = e_{33}^*/|e_{31}^*|$. The piezoelectric coefficients h_{3j}^* link mechanical strain and electric field due to the piezoelectric effect [24]. A large anisotropy of h_{3j}^* is achieved in a wide volume-fraction (m) range, and it is the common feature of the 1–3-type composites [21] with aligned piezoelectric rods. Comparing Eqs. (14) and (19), it is easy to show that the piezoelectric coefficient h_{33}^* and thickness ECF k_t^* are linked as follows:

$$k_t^* = h_{33}^*(\varepsilon_{33}^{*\xi}/c_{33}^{*D})^{1/2}. \quad (20)$$

A monotonic increase of the dielectric permittivity $\varepsilon_{33}^{*\xi}$ and elastic modulus c_{33}^{*D} from Eq. (20) on increasing the volume fraction of the piezoelectric rods (m in the case of the 1–2–2 composite) promotes similar configurations of the volume-fraction dependences of k_t^* and h_{33}^*, as is known from earlier studies (see, for instance, Refs. 21, 23 and 26).

Table 4 contains data on local maxima of h_{33}^* and k_t^* which are predicted for both the studied 1–2–2 composites. We can observe small differences between the maximum values of the parameter related to the araldite-containing and polyurethane-containing composites, Changes in the volume fraction m_s of *polymer I* in the laminar matrix do not lead to considerable changes in both k_t^* and h_{33}^*. This is mainly due to the relatively large volume fractions m_h and m_k at which local maxima of these parameters are achieved and at which the matrix does not strongly influence the piezoelectric properties of the 1–3-type composite. A comparison of the k_t^* and h_{33}^* values from Table 4 to the similar parameters of the KNNTL:Mn SC (see Table 1) enables us to state that an increase of k_t^* and h_{33}^* by approximately 1.9 and 1.4 times, respectively, is achieved in a wide m_s range. Such a high performance in the 1–2–2 composites studied here is important for piezoelectric sensor, energy-harvesting and transducer applications.

4 Comparison of results and discussion

This paper demonstrates that lead-free 1–2–2 composites reported here have a number of advantages over the composites based on the relaxor-FE SCs and FE ceramics. It can be seen from Table 5 that the composites based on the KNNTL:Mn SC exhibit large values of piezoelectric coefficients g_{33}^*, h_{33}^* and g_h^*, and the thickness ECF k_t^* which are achieved at relatively small volume fractions of SC m. The validity of conditions (12) and (13) and the large ani- sotropy of the squared figures of merit $(Q_{3j}^*)^2$ are also important characteristics that make the piezoelectric performance of the studied lead-free composites competitive in comparison to lead-containing composites based on the relaxor-FE SCs [21–23]. Among the factors that lead to these large parameters are the moderate dielectric permittivity $\varepsilon_{33}^{\sigma}$ of the KNNTL:Mn SC, the columnar architecture

Table 4 Local maxima of the piezoelectric coefficient h_{33}^* (in 10^{10} V·m^{-1}) and thickness ECF k_t^* of 1–2–2 composites at m_s = const

m_s	Local max h_{33}^*	Volume fraction m_h that corresponds to local max h_{33}^*	Local max k_t^*	Volume fraction m_k that corresponds to local max k_t^*
KNNTL:Mn SC / araldite / PE composite[a]				
0.05	1.53	0.855	0.937	0.571
0.10	1.53	0.846	0.936	0.551
0.30	1.51	0.821	0.930	0.505
0.50	1.50	0.806	0.924	0.489
0.70	1.48	0.794	0.916	0.493
0.90	1.47	0.780	0.901	0.540
KNNTL:Mn SC / polyurethane / PE composite[b]				
0.05	1.53	0.862	0.937	0.585
0.10	1.53	0.857	0.937	0.574
0.30	1.52	0.841	0.933	0.547
0.50	1.51	0.833	0.929	0.535

0.70	1.50	0.819	0.924	0.537
0.90	1.49	0.807	0.913	0.550

[a] For the KNNTL:Mn SC / araldite / PE composite, m_s is the volume fraction of araldite in the laminar matrix
[b] For the KNNTL:Mn SC / polyurethane / PE composite, m_s is the volume fraction of polyurethane in the laminar matrix

of the composite and the elastic anisotropy of its laminar matrix with interfaces oriented perpendicular to the poling axis OX_3 (see Fig. 1). The 1–2–2 composite based on the PMN–0.33PT SC is characterised by large squared figures of merit $(\mathcal{Q}_{33}^*)^2$ and $(\mathcal{Q}_h^*)^2$, see Table 5. Their volume-fraction behaviour, as follows from the analysis of Eqs. (6) and (7), is mainly due to the very large piezoelectric coefficients d_{3j} of the PMN–0.33PT SC, see Table 1.

Results of our evaluations of the effective properties of the 1–2–2 composite at m = const and m_s = const are compared to those obtained for a similar 1–2–2 composite with a system of cylindrical SC rods and with the same arrangement of the main crystallographic axes in each rod (see Section 2). In the second stage of our evaluations, we used the effective field method [21] to calculate the effective properties of the composite wherein the cylindrical rods were surrounded by the laminar matrix. Differences between the parameters evaluated for the composite shown in Fig. 1 and for its analog with cylindrical SC rods do not exceed 2% in the wide volume-fraction range. We add that an important comparison of effective parameters evaluated for a 1–2–2 composite based on a relaxor-FE SC by means of the matrix and finite element methods was carried out in work [22], where good agreement between the results was observed.

The studied 1–2–2 composites based on the KNNTL:Mn SC have no analogs among the three-component piezo-active composites [21, 22, 27, 28] due to the combination of the large parameters (e.g. g_{33}^*, h_{33}^* and g_h^*) and the large anisotropy of the piezoelectric coefficients and ECFs [valid conditions (12) and (13)]. The values of the piezoelectric coefficients g_{33}^* and g_h^* and related squared figures of merit $(\mathcal{Q}_{33}^*)^2$ and $(\mathcal{Q}_h^*)^2$ (Figs. 2–4) are a few times larger than the similar parameters of the 1–3-type, 2–2 and 3–3 composites based on FE ceramics of the PZT type [20, 28]. We add for a further comparison that the largest value of the thickness ECF k_t^* achieved in a 1–3 PMN–0.33PT SC / epoxy composite [29] is by 35% larger than k_t of its SC component.

In a 1–3-type composite wherein the PMN–0.33PT SC rods are surrounded by a porous araldite matrix, the effective parameters depend [23] on the volume fraction of SC and on the shape and volume fraction of air pores. For the case of heavily oblate spheroidal air pores with an aspect ratio 500 and porosity 30% in the araldite matrix, this composite is characterised by g_{33}^* = 522 and g_h^* = 459 (in mV·m·N^{-1}), $(\mathcal{Q}_{33}^*)^2$ = 1210 and $(\mathcal{Q}_h^*)^2$ = 934 (in 10^{-12} Pa^{-1}), and k_t^* = 0.943 [23]. Maximum values of h_{33}^* of a 1–3 PMN–xPT SC / araldite composite studied in work [23] vary from 0.261·10^{10} V·m^{-1} (at x = 0.30) to 0.569·10^{10} V·m^{-1} (at x = 0.42). In comparison to this performance, the 1–2–2 KNNTL:Mn SC / araldite / PE composite is characterised by larger values of g_{33}^*, g_h^* and h_{33}^*, see Tables 4 and 5. Moreover, a difference between values of max k_t^* of the 1–3-type PMN–0.33PT-based composite from work [23] and local max k_t^* of the 1–2–2 KNNTL:Mn-based composites (see Table 3) does not exceed 5%. It should be added that a 1–3 PMN–0.30PT SC / epoxy composite from work [30] is characterised by max $k_t^* \approx$ 0.8 (experimental), max g_{33}^* = 440 mV·m·N^{-1} at m_{SC} = 0.018 (calculated) and g_{33}^* = (80–120) mV·m·N^{-1} at m_{SC} = 0.25–0.70 (experimental). Here m_{SC} is the volume fraction of the [001]-poled PMN–0.30PT with the piezoelectric coefficient $d_{33} \approx$ 1500 pC·N^{-1} [30]. This d_{33} value is approximately 2.8 times

larger than d_{33} of the KNNTL:Mn SC (see Table 1), however the aforementioned max k_t^* and max g_{33}^* values are smaller than the similar parameters of the 1–2–2 composites, see data in Figs. 2 a, c and 3 a, c, and Table 4. As follows from experimental data [20] on 1–3 niobate FE ceramic / epoxy composite, its max $k_t^* \approx 0.5$ and max $g_{33}^* \approx 240$ mV·m·N^{-1} are also smaller than those predicted for the studied 1–2–2 composites. The piezoelectric coefficient d_{33} of the poled niobate ceramic [20] is approximately 2.5 times smaller than d_{33} of the KNNTL:Mn SC.

The 1–2–2 composites based on the KNNTL:Mn SC have advantages over various FE materials. According to experimental results [7], a nanostructured Mn-modified $(K_{0.5}Na_{0.5})NbO_3$ polycrystalline ceramic is characterised by the squared figure of merit $(Q_{33})^2 = 74.8 \cdot 10^{-12}$ Pa^{-1}. This value is smaller than those predicted for $(Q_{33}^*)^2$ of the 1–2–2 composites, see curves 1 and 3 in Fig. 4. However the anisotropy factor achieved for the Mn-modified $(K_{0.5}Na_{0.5})NbO_3$ ceramic [7] is $d_{33} / |d_{31}| \approx 21$, therefore, the ratio $(Q_{33})^2 / (Q_{31})^2 > 400$ is larger than $(Q_{33}^*)^2 / (Q_{31}^*)^2$ related to the composite, see Fig. 5. In a modified $PbTiO_3$ ceramic [1], the piezoelectric coefficients $d_{33} = 56$ pC·N^{-1} and $g_{33} = 33$ mV·m·N^{-1} are smaller than those achieved in the studied KNNTL:Mn-based composites, however the anisotropy factor $d_{33} / |d_{31}| = g_{33} / |g_{31}| = 8.2$ for the modified ceramic $PbTiO_3$ is comparable to the similar anisotropy factors of the KNNTL:Mn-based composites; for instance, see the 9th column in Table 5. As follows from data for the KNNTL:Mn-based composite at $m = 0.05$ and $m_s = 0.30$ (see the first part of Table 5), the anisotropy factor $g_{33}^* / |g_{31}^*| = 8.23$ is achieved at $d_{33}^* = 259$ pC·N^{-1} and $g_{33}^* = 1480$ mV·m·N^{-1}, i.e., we observe obvious advantages of the lead-free composite over the typical $PbTiO_3$-based ceramic from work [1]. A grain-oriented and highly textured modified $PbTiO_3$ material manufactured by Yan et al. [31] is characterised by the piezoelectric coefficient $g_{33} = 115$ mV·m·N^{-1}, and this value is by a few times smaller than g_{33}^* of the studied 1–2–2 lead-free composites, see Figs. 2 a, c and 3 a, c.

In Table 6 we show examples of the performance of the textured lead-free FE

Table 5 Comparison of effective parameters of 1–2–2 composites based on [001]-poled domain-engineered SCs

m	m_s	g_{33}^*, mV·m·N^{-1}	g_h^*, mV·m·N^{-1}	$(Q_{33}^*)^2$, 10^{-12} Pa^{-1}	$(Q_h^*)^2$, 10^{-12} Pa^{-1}	h_{33}^*, 10^{10} V·m^{-1}	k_t^*	$\frac{g_{33}^*}{\lvert g_{31}^*\rvert}$	$\frac{(Q_{33}^*)^2}{(Q_{31}^*)^2}$	$\frac{h_{33}^*}{\lvert h_{31}^*\rvert}$	$\frac{k_t^*}{\lvert k_p^*\rvert}$
KNNTL:Mn SC / araldite / PE composite											
0.05	0.10	1550	980	449	179	0.928	0.845	6.76	45.6	140	4.81
	0.20	1520	1020	416	186	0.910	0.835	7.81	60.9	103	4.80
	0.30	1480	1010	383	178	0.890	0.823	8.23	67.7	82.4	4.57
0.10	0.10	869	512	333	116	1.17	0.899	6.07	36.8	158	5.18
	0.20	862	537	318	124	1.16	0.894	6.88	47.3	115	5.04
	0.30	854	543	303	122	1.14	0.887	7.20	51.9	91.1	4.73
0.30	0.10	309	135	152	29.1	1.43	0.931	4.00	16.0	150	4.50
	0.20	309	143	149	32.2	1.42	0.929	4.26	18.2	109	4.09
	0.30	308	146	147	33.0	1.41	0.926	4.37	19.0	85.1	3.73
PMN–0.33PT SC / araldite / PE composite											
0.05	0.10	666	438	671	290	0.363	0.878	5.84	34.1	514	3.46
	0.20	655	455	613	295	0.362	0.870	6.51	42.4	372	3.38
	0.30	643	454	557	278	0.361	0.860	6.81	46.3	291	3.22
0.10	0.10	361	221	547	205	0.376	0.916	5.15	26.6	486	3.40
	0.20	358	231	513	214	0.375	0.911	5.65	32.0	353	3.24
	0.30	354	233	479	208	0.374	0.905	5.86	34.3	276	3.05
0.30	0.10	127	57.1	291	58.9	0.384	0.941	3.64	29.1	380	2.90
	0.20	187	104	367	114	0.384	0.932	4.52	20.5	276	2.93
	0.30	126	61.5	275	65.2	0.383	0.935	4.19	15.2	216	2.43

ceramics [32]. The g_{33} and $(Q_{33})^2$ values listed in Table 6 are smaller than the similar parameters of the studied 1–2–2 composites (see Figs. 2–4), and the piezoelectric coefficient d_{33} of the ceramics is comparable to d_{33}^* of the 1–2–2 composites at relatively small volume fractions of SC *m*.

5 Conclusion

We present the first detailed study of lead-free 1–3-type composites and their effective parameters for piezoelectric transducer and related applications. This includes the analysis of the piezoelectric properties and related parameters of lead-free composites with 1–2–2 connectivity, whose structure is shown in Fig. 1. The main piezo-active component is the [001]-poled KNNTL:Mn SC that exhibits large piezoelectric properties and electromechanical coupling, see data in Table 1. The SC rods in the composite sample are surrounded by the laminar polymer matrix with 2–2 connectivity. Such a matrix is of interest due to the elastic properties and their strong influence on the hydrostatic parameters and anisotropy factors of the 1–2–2 composite. The unique advantages of the studied 1–2–2 composites over conventional lead-based FE ceramic / polymer and modern relaxor-FE SC / polymer composites and many FE ceramics are the large values of the piezoelectric coefficients g_{33}^*, g_h^* and h_{33}^* and thickness ECF k_t^*, the large anisotopy of the squared figures of merit $(Q_{3j}^*)^2$, and the relatively large hydrostatic squared figures of merit $(Q_h^*)^2$.

Table 6 Room-temperature properties and squared figures of merit of poled textured $(K_xNa_{1-x})_{0.946}Li_{0.054}NbO_3$ ceramics[a]

x	d_{33}, pC·N^{-1}	$\varepsilon_{33}^{\sigma}/\varepsilon_0$	g_{33}, mV·m·N^{-1}	$(Q_{33})^2$, 10^{-12} Pa^{-1}
0.410	236	533	50.0	11.8
0.427	231	601	43.4	10.0
0.445	252	606	47.0	11.8
0.463	254	646	44.4	11.3

[a] From experimental results [32]

Conditions (12) and (13) for the large anisotropy of the piezoelectric coefficients and ECFs, respectively, are valid in specific ranges of the volume fractions *m* and m_s, see Fig. 7. It has been shown that the araldite / PE matrix with the larger difference of the elastic properties of *polymers I* and *II* leads to the simultaneous validity of conditions (12) and (13) as well as larger values of the piezoelectric coefficient g_h^* of the composite. Important correlations between the $s_{33}^{(m)}/s_{13}^{(m)}$ and d_{33}^*/d_{31}^* ratios and between the s_{anis} factor and k_t^*/k_p^* ratio (Table 3) have been initially found and described by interpretation of the validity of conditions (12) and (13) at $m << 1$ (Fig. 7), i.e., when an influence of the SC rods on the piezoelectric performance of the composite remains weak.

The presented parameters and advantages of the studied lead-free 1–3-type composites enable us to conclude that these materials can be used as active elements of modern piezoelectric sensors (with large g_{33}^*, $(Q_{33}^*)^2$, h_{33}^*, $(Q_{33}^*)^2/(Q_{31}^*)^2$, etc.), transducers and energy-harvesting devices (with large k_t^*. $k_t^*/|k_p^*|$, $d_{33}^*/|d_{31}^*|$, $(Q_{33}^*)^2$, and $(Q_{33}^*)^2/(Q_{31}^*)^2$), hydrophones (with large g_h^* and $(Q_h^*)^2$), and other piezotechnical devices.

Acknowledgements The authors would like to thank Prof. Dr. A. E. Panich and Prof. Dr. A. A. Nesterov (Southern Federal University, Rostov-on-Don, Russia) for their continuing interest in the research problems. Prof. Dr. C. R. Bowen would like to acknowledge funding from the European Research Council under the European Union's Seventh Framework Programme (FP/2007-2013) / ERC Grant Agreement no. 320963 on Novel Energy Materials, Engineering Science and Integrated Systems (NEMESIS). In the present paper, the results on the research project No. 11.1627.2017/4.6 PCh have been represented within the framework of the state task in the scientific activity area at the Southern Federal University, and Prof. Dr. V. Yu. Topolov acknowledges funding with thanks. This research has been performed using the equipment of the Centre of Collective Use 'High Technologies' at the Southern Federal University.

References

[1] Y. Xu, Ferroelectric Materials and Their Applications (North-

Holland, Amsterdam, London, New York, Toronto, 1991), pp. 108 –111, 131, 173–175.
[2] A. Safari and E. K. Akdogan (eds.), Piezoelectric and Acoustic Materials for Transducer Applications (Springer, New York, 2008), p. 59.
[3] S. Priya and S. Nahm (eds.), Lead-free Piezoelectrics (Springer, New York, Dordrecht, Heidelberg, London, 2012), p. 89.
[4] S. Priya and S. Nahm (eds.), Lead-free Piezoelectrics (Springer, New York, Dordrecht, Heidelberg, London, 2012), p. 139.
[5] L. Fu, D. Lin, Q. Zheng, X. Wu, and C. Xu. Phys. Stat. Sol. A **209**, 2299 (2012).
[6] Y. Huan, X. Wang, S. Zhang, R. Gao, and L. Li, Phys. Stat. Sol. A **210**, 2579 (2013).
[7] L. G. Gusakova, V. M. Poguibko, N. A. Spiridonov, V. M. Ishchuk, and N. K. Kisel', Nanosystems, Nanomaterials, Nanotechnologies **10**, 303 (2012, in Russian).
[8] L. M. Zheng, X. Q. Huo, R. Wang, J. J. Wang, W. H. Jiang, and W. W. Cao, CrystEngComm **15**, 7718 (2013).
[9] X. Huo, L. Zheng, R. Zhang, R. Wang, J. Wang, S. Sang, Y. Wang, B. Yang, and W. Cao, CrystEngComm **16**, 9828 (2014).
[10] X. Huo, R. Zhang, L. Zheng, S. Zhang, R. Wang, J. Wang, S. Sang, B. Yang, and W. Cao, J. Am. Ceram. Soc. **98**, 1829 (2015).
[11] W. Heywang, K. Lubitz, and W. Wersing (eds.), Piezoelectricity. Evolution and Future of a Technology (Springer, Berlin, 2008), p. 89.
[12] W. Heywang, K. Lubitz, and W. Wersing (eds.), Piezoelectricity. Evolution and Future of a Technology (Springer, Berlin, 2008), p. 131.
[13] R. Zhang, B. Jiang, and W. Cao, J. Appl. Phys. **90**, 3471 (2001).
[14] F. Levassort, M. Lethiecq, D. Certon, and F. Patat, IEEE Trans. Ultrason., Ferroelectr., a. Freq. Control **44**, 445 (1997).
[15] L. V. Gibiansky and S. Torquato, J. Mech. Phys. Solids **45**, 689 (1997).
[16] K. E. Evans and K. L. Alderson, J. Mater. Sci. Lett. **11**, 1721 (1992).
[17] Physics Encyclopaedia (Sovetskaya Entsiklopediya, Moscow, 1983, in Russian), p. 178.
[18] V. Yu. Topolov and C. R. Bowen, Mater. Lett. **142**, 265 (2015).
[19] R. E. Newnham, D. P. Skinner, and L. E. Cross, Mater. Res. Bull. **13**, 525 (1978).
[20] Z.-Y. Shen, Y. Xu, and J.-F. Li, J. Appl. Phys. 105, 104103 (2009).
[21] V. Yu. Topolov and C. R. Bowen, Electromechanical Properties in Composites Based on Ferroelectrics (Springer, London, 2009), pp. 29, 30, 46, 47, 52–56, 142–148.
[22] C. R. Bowen, V. Yu. Topolov, A. N. Isaeva, and P. Bisegna, CrystEngComm **18**, 5986 (2016).
[23] S. V. Bezus and V. Yu. Topolov, and C. R. Bowen, J. Phys. D: Appl. Phys. **39**, 1919 (2006).
[24] T. Ikeda, Fundamentals of Piezoelectricity (Oxford University Press, Oxford, New York, Toronto, 1990), pp. 16–20, 107–111.
[25] S. H. Choy, H. L. W. Chan, M. W. Ng, and P. C. K. Liu, Integr. Ferroelectrics 63, 109 (2004).
[26] H. L. W. Chan and J. Unsworth, IEEE Trans. Ultrason., Ferroelectr., a. Freq. Control **36**, 434 (1989).
[27] C. R. Bowen, V. Yu. Topolov, and H. A. Kim, Modern Piezoelectric Energy-harvesting Materials (Springer, Switzerland, 2016), pp. 24, 32, 61, 98–102.
[28] E. K. Akdogan, M. Allahverdi, and A. Safari, IEEE Trans. Ultrason., Ferroelectr., a. Freq. Control **52**, 746 (2005).
[29] K. C. Cheng, H. L. W. Chan, C. L. Choy, Q. Yin, H. Luo, and Z. Yin, IEEE Trans. Ultrason., Ferroelectr., a. Freq. Control **50**, 1177 (2003).
[30] F. Wang, C. He, and Y. Tang, Mater. Chem. Phys. **105**, 273 (2007).
[31] Y. Yan, J. E. Zhou, D. Maurya, Y. U. Wang, and S. Priya, Nature Communs **7**, 13089 (2016).
[32] J. Hao, C. Yo, B. Shen, and J. Zhai, Phys. Stat. Sol. A **209**, 1313 (2012).